Distant tail behavior during high speed solar wind streams and magnetic storms

C. M. Ho and B. T. Tsurutani
Jet Propulsion Laboratory, California Institute of Technology, Pasadena

Abstract. We have examined the ISEE 3 distant [ail data during three intense (Dst <-100 nT) magnetic storms and have identified the tail response to high-speed solar wind streams, interplanetary magnetic clouds, and near-Earth storms. The three storms have a peak Dst ranging from -150 to -220 nT and occur on January 9, February 4, and August 8, 1983, During [he storm onsets, the fast solar wind and magnetic field dynamic pressure ($B^2/8\pi + \sum n_i kT_i$) fluctuations moved the tail across the spacecraft multiple times. The magnetotail is strongly compressed by the outside sheath pressure. The lobe field strength can usually be predicted by the pressure balance. The strongest lobe field magnitude detected is 37 nT during storm main phase on January 10, which is higher than the sheath field by 5 - 10 nT. The sheath plasma pressure accounts for the higher lobe field strengths, However, for the February 4 storm, we find that three [ail lobe encounters are not in static balance with sheath pressure. During the storm times, the field magnitudes of the lobe and plasma sheet increase by a factor of 3-5 relative [o the quiet time. The temperature and density in both regions also increase by factors of 2-3, but with little plasma β changes, as one would expect. Under the assumption of tail flux conservation, increased sheath pressure implies a reduced tail size. Besides the tail size changes, the location of the nominal tail axis is controlled by solar wind flow orientation, This study shows that more than 70% of tail in-and-out events are predicted by either of these external mechanisms (changes of tail size due [o the external pressure and the solar wind directional changes). Nine tail plasma sheet jettings and 12 slow-mode shocks have been detected during the three storms. One remarkable feature of the jettings is very strong earthward flow (up to 1200 km/s) and tailward flow (up to 1500 km/s). The solar wind speed for these events was only -900 km/s, Both tail flow events have the highest speeds found to date. The preponderance of such a strong earthward flow indicates that during magnetic storms, magnetic reconnection occurs at locations well beyond the distance of ISEE 3. Through the interface of slow-mode shocks between the tail lobe and the plasma sheet/boundary layer, magnetic energy is being converted into plasma thermal and kinetic energy by the magnetic merging process. The predicted downstream plasma jetting speed (978 km/s) is consistent with the observations (1000 km/s) in the boundary layer. One surprising feature is that this reconnection process seems to be quite prominent during the storm recovery phase, One possible suggestion is that the dynamics of the distant tail are not at all related to magnetic storms and substorms but is an aftereffect, releasing extra magnetic tail energy by field sloughing via these reconnection events, accompanying the plasma sheet expansion.

1. Introduction

How the interplanetary parameters control the distant tail behavior is still not very well understood. *Fairfield [1993]* suggests that a long-duration northward interplanetary magnetic field (IM F) can result in a disappearance of the distant tail. Using ISEE 3 data, statistical studies from *Tsurutani et al.* [1986] show thar the tail lobe field strength is well correlated with the geomagnetic activity indices Kp and AE. The lobe field strength generally increases with increasing geomagnetic activity. Why such changes occur in the distant tail are not well understood, It is well known that if the IMF has a southward component, major magnetic flux erosion at the magnetopause will occur, with greater tail flaring and consequently greater tail compression as suggested by *Coroniti and* Kennel [1972]. On the basis of a flaring-tail model, *Tsurutani et al. [1986]* find that wirh erosion at the rnagnetopause and a large solar wind ram pressure, the flaring termination may reach a distance beyond 240 R_E, The tail field strength substantially increases inside 100 R_E, but essentially negligible changes at large distance > 140 R_E. Thus, increases in the distant tail field strength as a function of Kp and AE may be due to other reasons rather than near-Earth magneric merging,

Using recent Geotail data, the distant tail dynamics during magnetic storms, solar wind flow, and IMF variations have

been studied. *Nakamura et al. [1996]* show a case of magnetosheath encounter by Geotail near the center of the nominal tail axis during the main phase of a weak storm. *Kokubun et al.* (1996] have reported observations of magnetic field magnitudes as large as 53 nT in the distant tail during a moderate storm, In examining three ISEE 3 cases of long-duration magnetosheath encounters near the nominal tail axis, *Fairfield [1993]* finds that a stable and very northwardly directed IMF may be responsible for closing or even eliminating a distant tail. Thus for all parameters, such as solar wind pressure, IMF, and the occurrence of near-Earth magnetic storms and substorms, it is unclear which parameters are the dominanr ones in controlling the distant [ail characteristics.

Another long-standing topic which has been often debuted also is whether or not there are neutral lines in the distant tail (besides the near-Earth neutral line which causes substorms) and it' there are, what is their role for substorms. Also, the relationship of these distant neutral lines to those near-Earth are not well understood. Is the distant neutral line dependent on near-Earth geomagnetic activity, or is it always present'? During magnetic storms, are there more plasma jettings and more slow-mode shocks? If there are more, are they more intense? If dayside reconnection adds more field flux to the distant tail, then what is the effect of reconnection in the tail? All these questions need to be examined using distant tail data during major ($Dst < -100$ nT) magnetic storms.

In this study, we will examine all of the ISEE 3 distant tail passage data to select intervals of intense magnetic storms. During storm events, we will identify all of the various regions of the distant tail and compare them with more normal conditions, We will examine their dependence on solar wind conditions and phases of the magnetic storms. We will calculate plasma jetting speed based on a distant neutral line model and compare these results with observations. Finally, we will make some comparisons of our results with previous studies and discuss possible interpretations of these results.

2. Data

Using all of the ISEE 3 distant tail data, we have identified five intense ($Dst < -100$ nT) magnetic storms. Three storms have tail encounter data, while for the two other storms, the spacecraft unfortunately remained in the magnetosheath. We will study the three intense storms in this paper, The maximum Dst and a satellite location (in X ranges) for the events are listed in Table 1. The first two events take place during the first ISEE 3 distant tail pass, while the third comes from the second distant tail pass. The spacecraft trajectories for the three cases and its location relative to the tail axis are shown in Figure 1 in a GSE Y-Z plane (in this coordinate system, $\hat{X}$ points toward the Sun, $\hat{Y}$ is $\Omega \times \hat{X} / \lvert \Omega \times \hat{X} \rvert$, where Ω is the north ecliptic pole, and $\hat{Z}$ completes the right-hand system). To calculate a nominal tail axis, we have assumed a 4° aberration angle of the Earth's motion relative to a constant solar wind. An average location of X=215 R_E was assumed. A 15 R_E shift of the tail axis in the Y direction results from this correction.

The magnetic field measurements were obtained by the Jet Propulsion Laboratory magnetometer [*Frandsen et al., 1978].* This instrument measured 6 vectors per second, However, we have used l-rein averages of the field data for this study to match the resolution of the plasma data, The plasma observations presented here were obtained by the Los Alamos electron analyzer [*Bame et al.,* 1978]. Two-dimensional electron data are integrated over ±67.5° polar angle intervals centered on the spacecraft spin plane, which is nearly coincident with the ecliptic, Although a complete spectrum was measured in 3 s, consecutive measurements were taken only every 12 s. We have constructed l-rein averages of the plasma data for this study. The electron data used in this study include the electron density N_e, temperature T_e, and the two-dimensional plasma flow velocity V (V_x, V_y). The ion

measurement part of the instrument was not functional during the ISEE 3 distant tail passes.

3. Observations

3.1. Magnetic Field and Plasma Characteristics

From the examination of all distant tail measurements taken during the three storms, many large spike-like variations in the velocity, plasma density, and temperature can be noted (not shown) . These variations are indicative of multitail lobe, plasma sheet, and sheath encounters (this will redemonstrated later). Thus the data are a combination of observations in the magnetos heath, tail lobe, and plasma sheet. However, a clear trend can be seen in the magnetic field and velocity magnitudes during the storm main phase. This will help in the identification of the various regions within which the spacecraft is located, We thus first need to formulate criteria [o identify each region in detail before we can proceed [o characterize the properties of various tail regions during the storms.

On basis of previous studies [*Zwickl et al.*, 1984; *Slavin et al.*, 1985] and our recent/past experience [*Ho et al.*, 1994, 1996], the lobes, plasma s'beer, and sheath during quiet or substorm times are identified [o have the following characteristics. The tail lobes have stable magnetic fields (mainly in the B_x component, > 8 nT), lower plasma velocities (usually less than 200 km/s), the lowest plasma densities (< 0.2 cm^{-3}), intermediate temperatures (higher than the sheath. but lower than the plasma sheet: $1.2 \times 10^{6} > T_e > 6.5 \times 10^{5}$ K). The plasma sheet region is usually characterized by the lowest (< 2 nT) and most turbulent magnetic fields, B_x reversal, the highest temperatures ($T_e > 1.2 \times 10^{6}$ K), densities in the range from 0.2 to 1.0 cm^{-3}, and high plasma velocities (> 500 km/s). In contrast, the magnetosheath usually has cold temperatures (T_e < 6.5x 10^{5} K), high densities ($n_e > 1.0$ cm-3), turbulent fields, and a relatively constant solar wind speed (- 400 km/s). Using these criteria, we will examine data from all three storms, Because the second storm includes two main phases and is more complicated, we will study this event last. Thus we will study the three storms in an order of events 1, 3, and 2.

Figure 2 gives ISEE 3 distant tail observations for the first magnetic storm (January 9, 1983). From top to bottom are the *AE* and *Dst* indices, the three magnetic field components, field magnitude, two plasma velocity components. velocity magnitude, electron density, and temperature. During this storm, ISEE 3 was 33 R_E away from [he nominal tail axis (near the tail boundary), but only 2 - 4 R_E from the X-Y plane, ISEE 3 is in the magnetosheath for most of the time. At - 1600 UT, day 9, there is an interplanetary shock leading a solar ejects event, The shock (S) is identified by the abrupt jump in magnetic field magnitude from -6 to -16 nT, velocity from -400 to 600 km/s, density from 8 to 25 cm^{-3}, and temperature from ~2x10^{5} to -3x 10^{5}K, The IMF B_z is relatively steady, at a value near O nT, so the *Dst* response is only slight, There is a small southward component just behind the shock that causes a -1300 nT (*AE*) substorm.

A large southward turning in the field occurs at -0140 UT, day 10. This turning causes a substorm onset (SO) with -1200 nT in *AE*. *The* B_z configuration is southward then northward spanning an interval to -0400 UT, day 11. The magnetic field is smooth and relatively free of waves and discontinuities. We identify this as the driver gas of the solar ejects [*Tsurutani et al., 1988],* and the south-north rotation, a magnetic cloud [*Klein and Burlaga*, 1982]. The southward turning of the sheath field creates the main phase (MP) of the magnetic storm. The northward turning at -0900 UT day 10 leads to the start of the recovery phase (RP). The interplanetary interval from the shock to the driver gas creates the storm initial phase (1P). We have marked these intervals using vertical lines and letter abbreviations in Figure 2,

During the initial phase, two tail lobe encounters are detected, which have large B_x and $|B| > 20$ nT. The magnetic

storm (Dst --220 nT) is triggered by a stable and very large southward B_z (--25 nT). During the recover phase we see a strong negative B_y (-25 - -30 nT). At about 0900 UT, there is a tail lobe encounter which has the largest magnetic field (37 nT) magnitude we found, about 10 nT higher than the sheath field. During the tail encounter, [he plasma flow speed drops to < 200 km/s. The magnetic field shows very small B_y and B_z components. We do not see any plasma jetting events during this particular storm.

During the third magnetic storm (August 7,1983), ISEE 3 is located about -220 R_E in the distant tail, The distance from the nominal tail axis is between 12 and 14 R_E (inside the tail). All ISEE 3 observations are shown in Figure 3 with the same format as Figure 2. At 2100 UT, the solar wind speed jumps from 400 to 500 km/s. No obvious interplanetary shock and storm initial phase are identified. The storm main phase starts at 2,150 UT, when the magnetic field first turns southward accompanied by a large negative B_y (~-25 nT). The earliest tail encounter (northern tail lobe - 20 nT) is found at 2115 UT, only 10 min after a substorm onset. At 2240 UT, there is another transient southern tail lobe crossing. The field strength was 33 nT, which is higher than the sheath field by 2 -7 nT. The solar wind plasma pressure must account for the missing [ail pressure, At -0100 UT, August 8, B_z turns deeply southward again and B_y has also a reversal. At ~0700 UT, Dst reaches its maximum by 150 nT, and then a recovery phase starts immediately after B_z returns to -O nT. Other tail crossings are detected at around 0800 UT, The plasma bulk velocity usually drops to small values (< 200 km/s) for these tail encounters. During this storm, we see two earthward plasma a jettings with a speed of about +500 km/s. After 1400 UT, August 9, the spacecraft mainly stays inside the tail lobe and plasma sheet, We see many bidirectional (+500 to -S00 km/s) plasma flow events,

Compared to the first and third storms, the second storm event lasts much longer and has more tail crossings, Eight days of distant tail observations during the storm are shown in Figure 4 with the same format as before, An interplanetary shock occurs at 1700 UT, February 4, 1983, Around the shock there is a brief initial phase and a sudden impulse (S1). The southward field fluctuations after the shock trigger the storm main phase and substorm onset. However, closer inspection indicates that this storm consists of two main phases (MPa and MPb) and two recovery phases (RPa and RPb). Dst suddenly decreases [0-170 nT in the first main phase and then quickly recovers (RPa). When Dst returns to -100 nT, A large B_z southward turning causes the second main phase and another substorm onset at 0200 UT of day 36, Even though [his occurs exactly 26 days after the first magnetic storm, the high speed (- 900 km/s) solar wind stream and magnetic field have different features from the first storm on day 10. During the second main phase (MPb) of the storm, Dst decreases again to reach its minimum -185 nT. This storm then gradually recovers (RPb) to the normal values until day 42. During this recovering process, we can see many substorm events due to B_z southward fluctuations. The AE index has many peaks ranging from 500 to 2000 nT, Because there are so many tail encounters during this storm, these regions are not easily identified as in previous two storms. We need to use the criteria we developed to examine two days of storm data in high time resolution,

Figure 5a shows a 12 hour interval of data prior to the storm on February 4. 1983 during interplanetary quiet. At the top of Figure 5a is our legend, We have-used a blank box to represent the magnetosheath region, hatched box for the tail lobe, and black box for plasma sheet/boundary layer, During the 12 hours, AE is below 400 nT. the spacecraft is inside the tail most of time. The fields (B_x and B) are very stable (mostly in south lobe, ~-10 nT). The plasma speed irrside the tail is below 200 km/s, In contrast, in the magnetosheath the magnetic field is low (< 8 nT), and solar wind velocity is also stable at 400 km/s. The sheath plasma density is large (> 1 cm^{-3}).

During such quiet intervals we expect a clear pressure balance between the tail lobe and magnetosheath. The spacecraft occasionally crosses the plasma sheet, where there are high plasma temperatures and low fields. These are easily identifiable. During this period, lSEE 3 is about 11 R_E away from the nominal [ail axis (aberration corrected).

Figure 5b gives [he second 12 hours of data including [he first main phase (MPa) of storm 2. At 1610 UT, an interplanetary shock occurs. At the same time, a sudden impulse is detected at ground stations. This impulse causes the storm and substorm onsets. Then the spacecraft is in the sheath. The velocity, density and magnetic field all suddenly increase. The field B_z component has a southward turning and then a large fluctuation (± 15 nT) is followed. The-shocked plasma temperature increases from 2×10^5 to 6×10^5 K, The density increases from 5 to -60 cm^{-3}. The magnetic field magnitude jumps from 16 nT to -48 nT. The tailward plasma speed, V_{tw} (- *Vx),* also jumps to -1000 km/s. At 1640 UT around the shock, there is a 5-rein interval with very high temperature (2.0x 106 K) and low density. This region probably is a lobe crossing (also probably a plasma sheet crossing). After a data gap of 1730 - 2000 UT, we see that the spacecraft continuously stays inside the sheath. However, the storm quickly recovers because B,: becomes more northward,

In Figure 5c, we show the third 12 hours of data with the second main phase (MPb) of storm 2. The large interplanetary magnetic field with large $+B_z$ and -By components has a sudden southward B_z turning (from +25 to -23 nT) at 0200 UTof day 36. Then the stable southward IMF and MPb last at least 8 hours. The sheath high-speed stream has a constant tailward speed of - 1000 km/s. At 0235 UT the first tail lobe crossing after the storm onset is detected, We see a large B_x, high temperature, and reduced velocity and density during this lobe crossing, The interesting finding is that for this crossing the lobe field magnitude is significantly lower (by 13 nT) than outside the sheath. Even though the lobe field has a large B_x, its B_y and B_z components are much less than those inside the magnetosheath. We also find that two other lobe crossings occurring at 0410 and 0430 UT have lower fields than the adjacent sheath fields. The plasma densiry inside the lobe is 5-10 times Iower than outside sheath, while temperature is only 2-3 times higher [ban outside. Thus. this phenomenon is different from what weseen from storms 1 and 3. The difference suggests that temporally there is a total pressure unbalance between the sheath and the tail lobe. The high-density plasma and strong field will continue [o squeeze the tail until finally they both reach a balance. After 0430 UT, the tail lobe encounters show the lobe field magnitude higher than the sheath field, because IMF B_y and B: components inside the sheath have significantly decreased, Thus the pressures on both sides are balanced,

We see more plasma jetting and slow shock events in the last 12 hours shown in Figure 5d. Between 1930 and2000 UT, the earthward jetting has a speed as high as 1000 km/s. These jetting events are seen in the plasma sheet and lobe/boundary layer regions. Large tailward jettings with speeds greater than 1500 km/s are detected at 0630 and 1520 UT, These jettings show that reconnection processes are taking place in the distant tail. We will discuss these plasma Jetting and slow shock events later,

We summarize all characteristics for three distant regions during both storm and quite times in Table 2. These values are obtained by averaging the field and plasma parameters. There are 74 tail lobe encounters (54 during the storms), 9 plasma jetting events, and 12 slow-mode shocks from three storms. We find that during storms, the field magnitudes of the lobe and plasma sheet increase by a factor of 3-5 relative to the quiet time, The temperature and density in both regions also increases by a factor of 2-3. Thus there is an obvious increase in magnetic field intensity, plasma density, and temperature during storm times, as identified in previous studies [*Tsurutani et al., 1986].* However, the plasma β changes very little. The

changes are closely related [o changes in the field and plasma in the magnetosheath.

We also examine the correlation between the AE index and all tail lobe encounters, plasma jetting events, and slow-mode shocks, We find that there is a clear positive correlation between the lobe field magnitude and the AE index, However, the correlation between the earthward plasma jetting speeds in the plasma sheet and the AE index is not obvious. We see large jetting speed during both high and low AE intervals. We also examine the substorm dependence of the occurrence rates for these *events.* We use 10-min resolution *AE* index for [his study. All events of lobe crossings and plasma jettings inside the plasma sheet are identified to be present or not in each 10-min interval. Their occurrence rates are normalized by the total interval numbers. The statistical results are shown in Figure 6. In Figure 6a, we see that there are relatively more tail lobe crossings when the *AE index is* between 300 and 500 nT. This is mainly attributed to spacecraft's staying inside the tail lobe during late recovery phases of storms 2and 3, These events are detected in all *AE* intervals and all storm phases. Fourteen tail lobe encounters occur in [he storm main phase, while 40 appear during [he recover phase, In Figure 6b, we see that the occurrence of [he earthward jettings detected in the plasma sheet has no dependence on substorm activity. We have also used different lag times of AE index relative to the distant tail observations (from 20 to 40 rein). However, no obvious charge is seen for [heir occurrence rates, Plasma jettings are seen mainly (eight events) in the early recovery phase, while one in the main phase, Out of all nine jetting events, while seven correspond to substorms, two occur during lower *AE* (< *200* nT). However, the maximum lobe field strength detected seems to be related to the Dst (storm severity) magnitude, while jetting events seem to mainly occur during [he storm recovery phase.

3.2. Tail Pressure Balance and Solar Wind Aberration Effect

In order [o explain how the high-speed solar stream and magnetic storm affect the distant tail and why there are many tail/magnetosheath crossings during storm times, we need to examine both the changes ot tail size and tail flapping, For the former, we assume pressure balance between the sheath and tail lobe. Furthermore, if we assume tail magnetic flux conservation, the increasing tail field strength will result in a smaller tail, Thus when the sheath pressure increases, as a consequence, the spacecraft which would be originally within the tail may get into the sheath region, due to the tail compression, Then, in addition to an aberration angle due to Earth's motion relative to the solar wind V_x, the distant tail is also deflected due to variations of the solar wind speed V_y component (it is also possible that significant V_z variations deflect the tail, but these data are not available). Thus the tail axis will be strongly affected by both solar wind speed V_x and V_y. IMF B_y can twist the shape of tail but cannot significantly change the location of the tail. Tail flapping can explain those transit crossings between the tail and rnagnetosheath, but cannot explain the long intervals (several hours) within the tail or the sheath.

We first calculate the pressure balance between the sheath and the tail lobe during a high-speed stream. When the spacecraft is inside the magnetosheath, we may assume that the high sheath pressure squeezes the tail into a smaller region, During this time, for a steady state case, tbe outside sheath pressure will balance the inside tail lobe pressure. Neglecting the thermal pressure inside the tail (which is relatively small), we have

$$\frac{B_{\text{lobe}}^2}{8\pi} = \frac{B_{\text{sheath}}^2}{8\pi} + nkT \qquad (1)$$

Thus we may predict the lobe field magnitude from direct measurements of the magnetic field and plasma in the

magnetosheath. Furthermore, we assume the conservation of the lobe magnetic field flux; that is,

$$B_{lobe} R_{lobe}^2 = \text{const} \quad (2)$$

We used the previous statistical values [*Tsurutani et al., 1984; Slavin et al., 1985]* to determine the constant (when the lobe field has a magnitude of 11 nT, the tail has an average radius of $30 R_E$). Using the two equations we may calculate the lobe field and the corresponding tail size when the spacecraft is inside the sheath region. The calculated results for the three storms are shown in Figure 7. In Figure 7a, 7b, and 7c, we plot the measured magnetic field (solid line) which includes both sheath and [ail regions (we have shown the tail lobe encounters using shading). The dashed line is the predicted lobe field magnitude. We can see that the predicted lobe magnetic field is always larger than the sheath field, buthas a comparable strength with the measured lobe field. The magnetosheath field strengths have a broad range from 5 to 60 nT. The dashed lines are significantly higher than the sheath field. The difference is mainly due to larger sheath thermal (large plasma density) pressure.

The radius (or size) of the tail lobe based on the predicted lobe field are plotted in a dashed line in each lower panel in Figure 7. A smaller tail radius is clearly associated with a larger lobe field and larger sheath pressure, and vice versa. The [ail sizes may vary from 12 R_E *to* 40 R_E while the predicted lobe field varies from -50 nT in the peak of the compressed field region to 6 nT after this region, We see a gradual increase in the tail size accompanying this compressed region passover. The sizes after storms can even expand to larger than before the storms. For a reference, using a dotted line, we also plot the distance of the spacecraft from a tail axis which is only corrected by a fixed aberration (4") angle. Finally, we calculate a more accurate solar wind aberration angle, using measured velocities. We have used a solid line to plot the distance between rhe spacecraft and the corrected tail axis. When we calculate this distance, we use the solar wind speed V_x and V_y components measured only inside the magnetosheath. We see large variations of the distance from the corrected tail axis, due to large variations of solar wind velocity V_x and V_y. Using the relative variations between the dashed and solid lines, we can determine the spacecraft's position in the sheath or tail lobe. We can also compare this result with the location identified by the observations.

The solid tine going up and down relative to the dashed line suggests the spacecraft moving into and out of the tail lobe. We see that for most of the time when tail lobe encounters occur, the solid lines are below or close to the dashed lines. This shows that the spacecraft gets into the tail or detects the tail boundary. Overall, we find that the calculated locations are consistent with the observations 70% of the time. It suggests that the tail boundary location is controlled by both the sheath pressure and solar wind flow. However, we also find that the difference between the lines is large at some times (e.g., 1200-1600, day 009; 1300-2400 UT, day 010; 2000 UT of day 036-0200 of day 037; and 2000 UT of day 219-0100 of day 220). In the first three intervals, the calculations show that spacecraft should be inside the tail because its distance from the tail axis is less than the tail lobe radius, while the last one should be in the sheath, However, the observations show opposite situations. This inconsistency may be caused by the variations, of the solar wind speed V_x component (unfortunately, no measurements for this component are available), unstable tail magnetic flux (lack of flux conservation) during distant reconnection or a disappearing tail during a long interval of northward IMF (for *the* first two intervals). We note that the plasma jetting events are seen in the plasma sheet during two of the four intervals. It suggests that tail magnetic flux may not be a constant during the reconnection process in the distant tail. The size of the tail will no(change as we assumed during this time interval.

3.3. Plasma Jettings and Slow. Mode Shocks

During magnetic storms, some plasma sheet jetting and slow shock events are detected, This suggests that the distant neutral line or magnetic merging may exist beyond the 200 R_E distant tail, We do not see any jetting events at the first storm (January 10, 1983, spacecraft location seen in Figure 1), because very few tail encounters are seen during this storm. We see the jetting events in the other two storms. These jettings mainly appear during both storm main phases and recovery phases (when the spacecraft gets into the plasma sheet after 2000 UT of day 221 and 1200 UT of day 037, we see frequent plasma jettings). Most of these crossings between the tail lobe and the plasma sheet boundary layer/plasma sheet have been identified as slow shocks. Thus tail lobe magnetic energy has been converted into plasma kinetic and thermal energy in the plasma sheet through the interface of the slow-mode shock.

The highest earthward plasma jetting speed is -1200 km/s, which is detected at 0253 UT, day 037. This is also the highest speed of earthward plasma jettings ever found in the distant tail (upstream data not available). The second highest event (V_x = 1050 km/s) is seen at 1935 UT, day 036, Both earthward jetting events are detected in the recovery phase (RPb) of the second storm. In addition, some high speed tailward jettings (V_x <-*1500* km/s) also are detected. They are much larger than the magnetosheath flow speed (-900 - 1000 km/s). These events are the highest speeds we found to date.

The second highest earthward jetting event with high-resolution magnetic field data has been shown in Figure 8 in a GSE frame and rotated in a shock frame, respectively. By identifying each region, we see that the earthward flow mainly appears in the plasma sheet boundary layer region (in [he lobe side), instead of the plasma sheet region, Before 1925 UT, [he spacecraft is inside the sheath as we identified in Figure 5d. Then the spacecraft progressively crosses the south tail lobe, boundary layer (at 1945 UT). and plasma sheet (2000 UT). and then returns to the south lobe again at 2005 UT. In the Geotail study of Saito et al. [1995], they also find some earthward plasma flows in the lobe-like regions. We do not know whether or not these flows are due to leakage of plasma from the plasma sheet to the lobe, We have used [he coplanarity relation [e. g., *Colburn and Sonett, 1966] to* calculate the shock normal. All measured parameters are listed in Table 3, They include the upstream average magnetic field B_u, downstream field B_d, and N_e, T_e, and V for both the upstream and downstream regions, In [his shock reference system, "downstream" is the boundary layer with high speed earthward *flow* and plasma sheet bounded by the first pair of vertical lines, and "upstream" is the tail lobe bounded by the second pair of vertical lines. Both the upstream and downstream magnetic fields are rotated into a shock normal coordinate system. Along the shock normal, there is a significant B component (B_n = -5.23±1.21 nT) across the shock. The maximum errors in the magnetic field are derived from the standard deviations of the upstream and downstream field values,

We have defined some magnetic field angles in the following to compare with the *Petschek [1964]* model. We have sketched the geometry of the magnetic neutral line and earthward slow shock in Figure 9. At first, we project the magnetic field and the shock normal into the *x-z* plane, There is a angle θ_{nz} between the normal n and the z axis, where θ_{nz} = $\cos^{-1}$ n. The second angle is ξ between the shock normal in the x-z plane and the z axis, where $\xi = \tan^{-1} n_x/n_z$. The third angle is η, between the shock normal n in the x-z plane and the field B in the x-z plane, that is, $\eta = \cos^{-1} \bar{B}_{xz} \cdot \bar{n}_{xz} / |\bar{B}_{xz}||\bar{n}_{xz}|$. The fourth angle χ, lies between the magnetic field line in the x-z plane and the x axis. The angle $\tilde{\chi}$ is the acute angle of $\eta - \xi$. We next use the Rankine-Hugoniot conservation relations to calculate the plasma flow velocity along the normal direction in the upstream region

under the assumption of the conservation of B_n, mass, tangential electric field, and momentum [*Ho et al.*, 1996]. All calculated angles and speeds are shown in Table 3. For [his case, the plasma flow velocity along [he normal, V_{un} is greater than the slow-mode speed V_{sl} and less than the Alfven speed in the normal V_{An}, as expected for a slow mode shock.

Then, based on the theory of *Hill [1975]* and *Vasyliunas* [1975], the outgoing plasma jetting speed in the plasma sheet, V_{xd} is

$$V_{xd} = V_{Au} \cos\chi = V_{Au} \sin(\eta - \xi) \quad (3)$$

Using the Alfven velocities V_{Au} and angles listed in Table 3, we obtain an earthward plasma sheet V_{xd} of 987±45 km/s for this shock. This speed calculated from the theoretical model is consistent with the measured jetting speed (1002 km/s). Thus this confirms the existence of a Petschek type of neutral line. High-speed jetting flow is the result of reconnection in the distant tail. This result is also consistent with boundary layer plasma jettings in the picture of *Cowley et al.* [1984].

4. Discussion

In [his section, we will compare our results with previous studies and discuss possible explanations for these results. *Kokubun et al.*[1996] find that most large tail events seen by Geotail occur during main phases of storms, We also see these large [ail field events in main phases of storms. We think that this is because high-speed solar wind streams and magnetic clouds (large external pressure) occur in these phases of storms. The increase of field strength inside the tail is mainly related to an increase in outside sheath pressure, not the near-Earth geomagnetic activity, We also note that enhanced sheath thermal pressure is always accompanied by enhanced dynamic pressure in the solar wind. However, the effect of dynamic pressure is very small because the flaring angle of the tail boundary is very small in the distant [ail,

After an instantaneous solar wind aberration correction, *Nakamura et al, [1996]* find that all five cases are distributed around the magnetopause boundary (between the rwo lobe radii of 24 and 29 R_E). In a recent study, *Williams et al. [1994]* find that the magnetosheath encounters are consequences of solar wind aberration effects, However, our study shows that more than 20% of the time the spacecraft locations relative to the [ail cannot simply be interpreted by the solar wind (V_x and V_y) aberration effect. *Kokubun et al. [1996]* list '23 large tail (> 20 nT) field events detected by Geotail during magnetic storms, They find that the unusual strongest lobe encounter (53 nT) cannot be explained in terms of solar wind aberration and external pressure, unless the magnetic flux increase dots not reduce [he tail radius, We find during two intervals of stable northward B_z the spacecraft is in [he magnetosheath, even though its location is very close to the nominal tail axis, The long stable northward IMF may cause disappearing of the distant [ail as proposed by *Fairfield* [1993] or a filament tail structure,

Actually, dayside magnetic merging during the southward lMF may cause a magnetic flux increase in the near tail, During the expansion phase of a substorm, the tail flux will decrease due to the near-Earth reconnection *[Baker et al.,* 1987]. These changes will not be directly related to the sheath pressure. Thus the changes of tail size cannot be deduced based on the flux conservation under this situation, As in the case we see during the' second storm (at -0600 UT, day 36), there is an obvious unbalance between the lobe and the sheath in total pressures. If a reconnection occurs in the distant tail during this time, the tail lobe field flux may not be constant. The tail size will rapidly change to reach a steady state, As a result, we see some plasma sheet crossings which are associated with earthward plasma jetting and slow-mode shocks at 0535 UT or later. Various models have been proposed to explain how the

magnetic flux is added and then is cut off during [he dayside magnetopause reconnection,

Another reason may be that the magnetic tail is not cylindrical as we assumed in Figure 1. The [ail often is twisted or deformed by the IMF B_y effect [*Sibeck et al.*, 1985]. We have also detected vet-y large B_y (-30 nT) in our three storm events. Thus [he changes related [o IMF variations would also cause multicrossings when the spacecraft is near the nominal magnetopause. Recent global MHD simulation shows that most magnetosheath encounters may be due to IMF rotations from northward to duskward [*Frank et al.*, 1995], however, tail twisting and flattening can only explain transient crossings, near [o the magnetopause.

Magnetosheath encounters reported by *Nakamura et al.* [1996] have a timescale of 2 - 18 rein, while the magnetic [ail lobe encounters reported by *Kokubun et al. [1996]* have - 20-min duration, In our study we find that most tail lobe encounters have a duration from 10 min [o 1 hour and the separation between two encounters is 2 - 3 hours. These have been explained due to magnetopause surface waves related to solar wind oscillation [*Sibeck et al.*, 1985].

For those high-speed plasma jetting events, because their speed is far higher than the sheath solar wind flow, a reconnection process should occur in the distant tail, However, the question is whether or not these distant neutral lines are always present (independent of magnetic storms and solar wind) and do they have any relationship with a near-Earth neutral line. We suggest that a distant neutral line which is independent of the near-Earth neutral line probably always exists, *Ho et al.* [1994] have reported a near-complete distant reconnection case which includes a pair of slow-mode shocks, bidirectional plasma flows and plasma sheet B_z reversals. Because some such signatures are detected during northward IMFs, Ho *and Tsurutani* [1995] have proposed a model to explain [he distant neutral line formation during both northward and southward B_z situations.

These plasma jetting events mainly occur after a magnetic field compression process. It is possible that some external solar wind energies are transferred into [he tail though the compression process or other unknown paths (e. g., the opening of the tail) during main phase. After storm these energies stored inside the plasma sheet are released as the plasma jetting signatures. Also, during recovery phase. both the sheath and tail lobe fields become very low (- 5 nT, even lower than that before the storm). We expect that there is a tail expansion under such low field strength, This makes easily for the spacecraft to enter the plasma sheet and to detect these jetting flows. We have seen that the spacecraft goes back and forth between the tail lobe and the plasma sheet boundary layer/plasma sheet, Bidirectional jetting flows are detected during two magnetic storms (storms 2 and 3). For the first storm we do not see any jetting. The spacecraft may not get into the plasma sheet deep enough.

5. Summary

We have examined the ISEE 3 distant tail data during the five strongest magnetic storms (Dst < -100 nT) and identified the tail signatures with high-speed solar wind streams, magnetic clouds and near. Earth storms. Three of the storm events with obvious distant tail encounters have been studied in detail. We have characterized the field and plasma parameters in the different tail regions during both storm and quiet times.

1, During the storm onsets the strong solar wind and magnetic field fluctuations move the tail back and forth across the spacecraft, The lobe field strengths may be predicted under an assumption of the balance between the inside tail lobe magnetic pressure and outside sheath thermal and magnetic pressure,

2. During storms the distant tail is strongly compressed by the outside sheath pressure. The field magnitudes in the lobe and plasma sheet increase by a factor of 3-5 relative to quiet

times. The temperature and density in both regions also increases by a factor of 2-3, while plasma β changes very little, as expected,

3. The strongest magnitude of lobe field we detected during a storm main phase is 37 nT (January 10), which is higher than the sheath field by 5 -10 nT. However, three tail lobe encounters, seen also during main phases, show a pressure unbalance between [he lobe (lower field B and plasma density) and the adjacent sheath, It may suggest that the tail is unstable or developing during these intervals.

4. Except for the tail size changes due to field strength changes under an assumption of the tail flux conservation, we also find that the orientation of nominal tail axis is strongly affected by solar wind speed V_y and V_x components. More than 70% of [ail crossing events may be predicted by the changes of tail size due to the pressure balance and solar wind directional changes. The remaining cases may be caused by the effect of solar wind V_z and flux changes due to reconnection.

5. Nine tail plasma sheet jettings and slow-mode shocks have been detected in the second and third storms. One remarkable feature of [he jettings is very strong earthward (up to 1200 km/s) and tailward flows (1500 km/s compared to 900 km/s solar wind speed), and quasiperiodic (- 3 hour) characteristics. The preponderance of such earthward flowing events indicates that during magnetic storms, magnetic reconnection is occurring at locations well beyond the distance of ISEE 3,

6. Through the interface of slow-mode shocks between the tail lobe and the plasma sheet/boundary layer, the magnetic energy is converted into plasma thermal and kinetic energy by the magnetic merging process, The calculated plasma jetting speed (987 km/s) based on a Petschek slow shock model is consistent with observations (1000 km/s) in the boundary layer.

7. Plasma sheet plasma jetting events are mostly detected during the recovery phases of the storms, when the heated plasma sheet expand under a reduced sheath pressure. These plasma jetting events are probably independent of near-Earth reconnection and AE index. However, during the storms, because the distant tail is compressed by the high-speed solar wind streams, some external energies may be transferred and stored inside the tail through some unknown mechanisms. As an aftereffect, these extra magnetic tail energies is released by field sloughing via these reconnection events,

Acknowledgments: The research conducted at the Jet Propulsion Laboratory, California Institute of Technology was performed under contract [o the National Aeronautics and Space Administration,

The Editor thanks S .J. Schwartz and another referee for their assistance in evaluating this paper,

References

Baker, D.N, R.C. Anderson, R.D. Zwickl, and J.A. Slavin, Average plasma and magnetic field variations in the distant magnetotail associated with near-Earth substorm effects, *J. Geophys. Res.*, 92, 71, 1987.

Bame, S. J., J.R. Asbridge, H.E. Felthauser, J.P. Gore, G. Paschmann, P. Hemmerich, K. Lehman, and H. Rosenbauer, ISEE-1 and ISEE-2 fast plasma experiment and the ISEE 3 solar wind experiment, *IEEE Trans. Geosci. Electron., GE-16, 216, 1978,*

Colburn, D. S., and C.P. Sonnett, Discontinuities in the solar wind, *Space Sci. Rev., 5,* 439, 1966.

Coroniti, F. V., and C.F. Kennel, Changes in magnetospheric configuration during the substorm growth phase, *J. Geophys. Res., 77, 3361,* 1972.

Cowley, S.W.H., 'E'he distant geomagnetic tail in theory and observation, in *Magnetic Reconnection in Space and Laboratory Plasma, Geophys. Mongr. Ser.,* Vol., 39, Edited by E.W. Hones Jr., p228, AGU, Washington, D.C, 1984.

Fairfield, D. H., Solar wind control of the distant magnetotail: ISEE 3, J. *Geophys. Res.,* 98, 21265, 1993.

Frandsen, A. M. A., B.V. Connor, J, Van Amersfoort, and E.J. Smith, The ISEE-c vector helium magnetometer, IEEE *Trans. Geosci. Electr.,* GE-16, 195, 1978.

Frank, L. A., et al., observations of plasma and magnetic field in Earth distant magnetic tail: Comparison with a global MHLJ model, *J. Geophys. Res., 100,* 19177, 1995.

Hill, T. W., Magnetic merging in a collisionless plasma, *J. Geophys. Res., 80,* 4689, 1975.

Ho, C.M., and B.T. Tsurutani, Distant tail plasma jetting and B_z properties at slow-mode shocks: A model of reconnection during northward IMFs, *Geophys. Res. Lett., 22,* 2977, 1995.

Ho, C. M., B.T. Tsurutani, E.J. Smith, and W.C. Feldman, A detailed examination of a X-line region in the distant tail: ISEE 3 observations of jet flow and B_z reversals and a pair of slow shocks, *Geophys. Res. Lett., 21,* 3031, 1994.

Ho, C.M., B.T. Tsurutani, E.J. Smith, and W.C. Feldman, Properties of slow-mode shocks in the distant (>200 R_E) geomagnetic tail, *J. Geophys. Res., 101,* 15277, 1996,

Klein, L. W., and L.F. Burlaga, Interplanetary magnetic clouds at 1 AU, *J. Geophys. Res.,* 87, 613, 1982.

Kokubun, S., L.A. Frank, K. Hayashi, Y. Kamide, R.P. Lepping, T. Mukai, R. Nakamura, W.R. Paterson, T. Yamamoto, and K, Yumoto, Large field events in the distant magnetotail during magnetic storms, *J. Geomagn. Geoelectr., 48,* 561, 1996.

Nakamura, R., et al., observations of the magnetosheath near the nominal [ail axis during the geomagnetic storm of January 25, 1993, *J. Geomagn. Geoelectr.,* 48, 577, 1996.

Petschek, H. E., Magnetic field annihilation, in *AAS-NASA Symposium on the Physics of Solar Flares,* edited by B'. X. Hess, *NASA Spec. Publ., 50,* 425, 1964.

Saito, Y., T. Mukai, T, Terasawa, A. Nishida, S, Machida, M. Hirahara, K. Maezawa, S. Kokubun, and T. Yamamoto, Slow-mode shock in the magneto tail, *J. Geophys. Res., 100,* 23567, 1995,

Sibeck, D, G., G.L. Siscoe, J.A. Slavin, E.J. Smith, B.T. Tsurutani, and R.P. Lepping, The distant magnetotail's response to a strong interplanetary magnetic field B_y: Twisting, flattening, 'and field line bending, *J. Geophys. Res.,* 90, 4011, 1985,

Slavin, J. A., E.J. Smith, D.G. Sibeck, D.N. Baker, R.D. Zwickl, and S,-1. Akasofu, An ISEE 3 study of average and substorm conditions in the distant magneto tail, *J. Geophys. Res.,* 90, 10875, 1985,

Tsururani, B, T., J.A. Slavin, E.J. Smith, R. Okida, and D.E. Jones, Magnetic structure of the distant Geotail from -60 to -220 R_E: ISEE 3, *Geophys. Res. Lett., 11, 1,* 1984.

Tsurutani, B, T., B. El. Goldstein, M.E. Burton and D.E. Jones, A review of the ISEE 3 Geotail magnetic field results, *Planet. Space Sci.,* 34, 931, 1986.

Tsurutani, B, T., W.D. Gonzalez, F, Tang, S.1, Akasofu, and E.J. Smith, Origin of interplanetary southward magnetic fields responsible for major magnetic storms near solar maximum (1978-1979), *J. Geophys. Res.,* 93, 8519, 1988.

Vasyliunas, V. M., Theoretical models of magnetic field line merging, 1, *Rev. Geophys., 13, 303, 1975,*

Williams, D. J.. et al.. Magnetopause encounters in [he magnetotail at distances of -80' R_E, *Geophys. Res. Lett.,* 25, 3007, 1994.

Zwickl, R.D., D.N. Baker, S.J. Bame, W.C. Feldman, J.T. Gosling, E.W. Hones Jr., and D.J. McComas, Evolution of the Earth's distant magnetotail: ISEE 3 electron plasma results, *J, Geophys. Res.,* 89, 11,007, 1984.

C.M. Ho, and B. T, Tsurutani, MS 169-506, Jet Propulsion Laboratory, California Institute of Technology, 4800 Oak Grove Drive, Pasadena, CA 91109 (email: cho@jplsp.jpl.nasa.gov)

HO AND TSURUTANI: DISTANT TAIL DURING MAGNETIC STORMS

HO AND TSURUTANI: DISTANT TAIL DURING MAGNETIC STORMS

HO AND TSURUTANI: DISTANT TAIL DURING MAGNETIC STORMS

HO AND TSURUTANI: DISTANT TAIL DURING MAGNETIC STORMS

HO AND TSURUTANI: DISTANT TAIL DURING MAGNETIC STORMS

HO AND TSURUTANI: DISTANT TAIL DURING MAGNETIC STORMS

HO AND TSURUTANI: DISTANT TAIL DURING MAGNETIC STORMS

HO AND TSURUTANI: DISTANT TAIL DURING MAGNETIC STORMS

HO AND TSURUTANI: DISTANT TAIL DURING MAGNETIC STORMS

HO AND TSURUTANI: DISTANT TAIL DURING MAGNETIC STORMS

HO AND TSURUTANI: DISTANT TAIL DURING MAGNETIC STORMS

HO AND TSURUTANI: DISTANT TAIL DURING MAGNETIC STORMS

(Received May 27, 1996; revised October 9, 1996; accepted October 28, 1996.)

Paper number 96 JA03872.
0148 -0227 /97/96 JA-03872$09.00

Figure Captions

Figure 1. ISEE 3 locations relative to the tail axis during three magnetic storms in Y-Z plane ([ail cross section). The center of the tail has a -15 R_E shift in $+Y$ direction after an aberration (~4°) correction. Tail section is approximately shown as a cylindrical with - 30 R_E radius. On basis of this sketch, two cases occur inside [he tail. while one case is seen near the tail boundary, though exact location relative to the tail much depend on solar wind flow and the size variations.

Figure 2. ISEE 3 observations *Of* magnetic field and plasma in [he distant tail during magnetic storm on January 9- 13, 1983. Top two panels give near-Earth substorm (AE) and storm (Dst) indices, A large high-speed solar wind stream and magnetic cloud last more than two days, Five tail lobe crossings with very strong field strength are identified, Before the storm main phase, large sheath pressure has cause the increase of lobe field.

Figure 3. A magnetic storm occurred on August 7 - 11, 1983, and the distant tail observations. During this period the solar wind flow speed does not increase much. However, magnetic cloud B_z turns southward twice. We see many tail lobe crossing and plasma jetting events in the recovery phase,

Figure 4. A long-duration magnetic storm with two main phases and the distant tail measurements. Solar wind speed increases significantly from -450 to -900 km/s, while the sheath field reach a value as large as - 45 nT. Many tail crossings and plasma jetting are seen during main and recovery phases.

Figure 5. A detail identification of each distant tail region with high resolution data, Two days of data are divided into four plots: (a) prestorm; (b) first storm onset; *(c)* second storm onset, and (d) early recovery phase. Three regions are marked out: blank, magnetosheath; hatched, tail lobe; and black, plasma sheet.

Figure 6. AE dependence of [he occurrence rates of (a) tail lobe crossings and (b) plasma sheet earthward plasma jettings. There are relatively more tail lobe crossings when AE index is between 300 and 500 nT, which is mainly attributed to tail lobe staying during late recovery phases of storms 2 and 3, earthward jetting events have no dependence on substorm activity. There are no obvious changes for different lag times of AE index relative *lo* the tail observations,

Figure 7. Pressure balance between the sheath and tail lobe and spacecraft relative location to the tail center for three magnetic storms. Solid line give the distance of spacecraft relative to a solar wind aberration corrected tail axis. Dashed line give the tail size which varies depending on predicted tail field strength under an assumption of tail flux conservation. Dotted line is the distance from a tail center which just corrected by a fixed aberration (4°) angle. A relative Variation of the solid line to the dashed line will show how spacecraft gets in and out from the tail.

Figure 8. A strong plasma jetting and slow-mode shock event detected around 2000 UT, February 5, 1983. Magnetic field also is rotated into a shock frame (B_i, B_j and B_k). earthward plasma flow is detected in the region of plasma sheet boundary layer, We have identified the interface between the lobe and plasma sheet as a slow-mode shock using coplanar theorem and R-H relation.

Figure 9. A sketch to show the geometry of slow-mode shock and plasma jetting location The spacecraft entry from and exit into the south lobe across [he slow-mode shock and boundary layer earthward the neutral line. All shock parameters are calculated and compared with the real measurements.

Figure 1. ISEE 3 locations relative to the tail axis during three magnetic storms in Y-Z plane (tail cross section). The center of the tail has a -15 R_E shift in $+Y$ direction after an aberration (-4°) correction. Tail section is approximately shown as a cylindrical with - 30 R_E radius. On basis of this sketch, two cases occur inside the tail, while one case is seen near the tail boundary, though exact location relative to the tail much depend on solar wind flow and the size variations.

Figure 2. ISEE 3 observations of magnetic field and plasma in the distant tail during magnetic storm on January 9 - 13, 1983. Top two panels give near-Earth substorm (AE) and storm (Dst) indices. A large high-speed solar wind stream and magnetic cloud last more than two days. Five tail lobe crossings with very strong field strength are identified, Before the storm main phase, large sheath pressure has cause the increase of lobe field.

Figure 3. A magnetic storm occurred on August 7 - 11, 1983, and the distant tail observations. During this period the solar wind flow speed does not increase much. However, magnetic cloud B_z turns southward twice. We see many tail lobe crossing and plasma jetting events in the recovery phase.

Figure 4. A long-duration magnetic storm with two main phases and the distant tail measurements. Solar wind speed increases significantly from -450 to -900 km/s, while the sheath field reach a value as large as - 45 nT. Many tail crossings and plasma jetting are seen during main and recovery phases.

Figure 5. A detail identification of each distant tail region with high resolution data. Two days of data are divided into four plots: (a) prestorm; (b) first storm onset; (c) second storm onset, and (d) early recovery phase, Three regions are marked out: blank, magnetosheath; hatched, tail lobe; and black, plasma sheet.

Figure 6. AE dependence of the occurrence rates of (a) tail lobe crossings and (b) plasma sheet earthward plasma jettings. There are relatively more tail lobe crossings when AE index is between 300 and 500 nT, which is mainly attributed to tail lobe staying during late recovery phases of storms 2 and 3. earthward jetting events have no dependence on substorm activity. There are no obvious changes for different lag times of AE index relative to the tail observations.

Figure 7. Pressure balance between the sheath and tail lobe and spacecraft relative location to the tail center for three magnetic storms. Solid line give the distance of spacecraft relative to a solar wind aberration corrected tail axis. Dashed line give the tail size which varies depending on predicted tail field strength under an assumption of tail flux conservation. Dotted line is the distance from a tail center which just corrected by a fixed aberration (4°) angle. A relative variation of the solid line to the dashed line will show how spacecraft gets in and out from the tail,

Figure 8. A strong plasma jetting and slow-mode shock event detected around 2000 UT, February 5, 1983. Magnetic field also is rotated into a shock frame (B_i, B_j and B_k). earthward plasma flow is detected in the region of plasma sheet boundary layer. We have identified the interface between the lobe and plasma sheet as a slow-mode shock using coplanar theorem and R-H relation.

Figure 9. A sketch to show the geometry of slow-mode shock and plasma jetting location. The spacecraft entry from and exit into the south lobe across the slow-mode shock and boundary layer earthward the neutral line. All shock parameters are calculated and compared with the real measurements,

Table 1. Three Magnetic Storm Data Interval, *Dst* and ISEE 3 Trajectory Coverage

Storm Events	Data Intervals	Maximum *Dst*, nT	Trajectory Ranges. R_E
Case 1	day 009-013, 1983	-220	-166.8 > X >-181.5
Case 2	day 034-042, 1983	-185	-219.5 > X > -219.9
Case 3	day 219-223, 1983	-150	-221.6 > X >-217.9

Table 2. Distant Tail Parameters During Storm and Quiet Times

Time	Regions	|B|, nT		N., cm-'		T_p, K		V, km/s		β Rate	
		Storm	uite	Storm	Quite	Storm	uite	Storm	Quite	Storm	Quite
January	MS	27	10	22.0	5.0	3. OX1O'	1.5x10³	600	450	0.31	0.26
9-13,	tail lobe	37	8	1.0	0.5	8.0x10⁵	4. OX1O5	250	150	0.02	0.11
1983	PS	8	3	0.5	0.2	I.3X106	I. 0x10⁶	750	500	0.35	0,77
February	MS	45	7	40.0	8.0	0.6x10⁷	O.2X1O'	900	500	0.43	0.35
3-10,	tail lobe	28	12	0.2	0.1	1. OX1O6	O,7X1O6	600	300	0.01	0.01
1983	PS	5	2	0.6	0.1	3.5X106	1.5x10⁶	1300	800	2.90	1.30
August	MS	25	10	20.0	6.0	2. OX1OJ	I. OX1OJ	500	400	0.22	0.20
7-11,	tail lobe	31	14	2.0	0.5	6.0x10⁵	5.0x10⁵	200	150	0.04	0.04
1983	PS	8	2	0.2	0.1	1.5x10⁶	1.0x10⁶	1 000	800	0.16	0.87

MS, magnetosheath; PS, plasma sheet.

Table 3. Plasma Jetting and Slow-mode Slow Parameters

Parameter	Value
B_u, nT	-8.30, -0,03, 0.54
B_d, nT	-0.26, -4.24, -0.53
B_n, nT	-5.23
V_u, km/s	210
V_d, km/s	940
Shock Normal, *n*	-0.38, 0.27, 0.89
n_u, cm^{-3}	0.02
n_d, cm^{-3}	0.04
T_u, K	1.5X106
T_d, K	3, OX1O6
θ_{Bnu}, deg	71.5
θ_{Bnd}, deg	38,8
θ_{nz}, deg	27.6
ξ, deg	21.2
η, deg	70.6
V_{Au}, km/s	1300
V_{Aun}, km/s	862
V_{nu}, km/s	576
V_{sl}, km/s	243
M_{An}	0.68
β	0.05

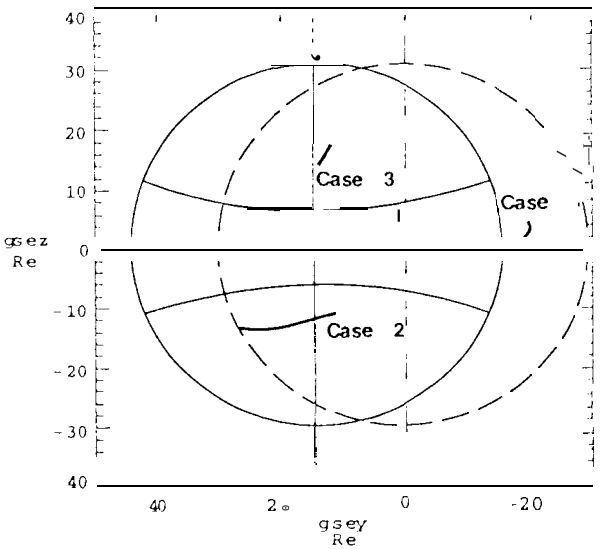
40
30
20
10
0
-10
-20
-30
40
gsez
Re
Case 3
Case
Case 2
40
20
0
-20
gsey
Re

Fig. 1

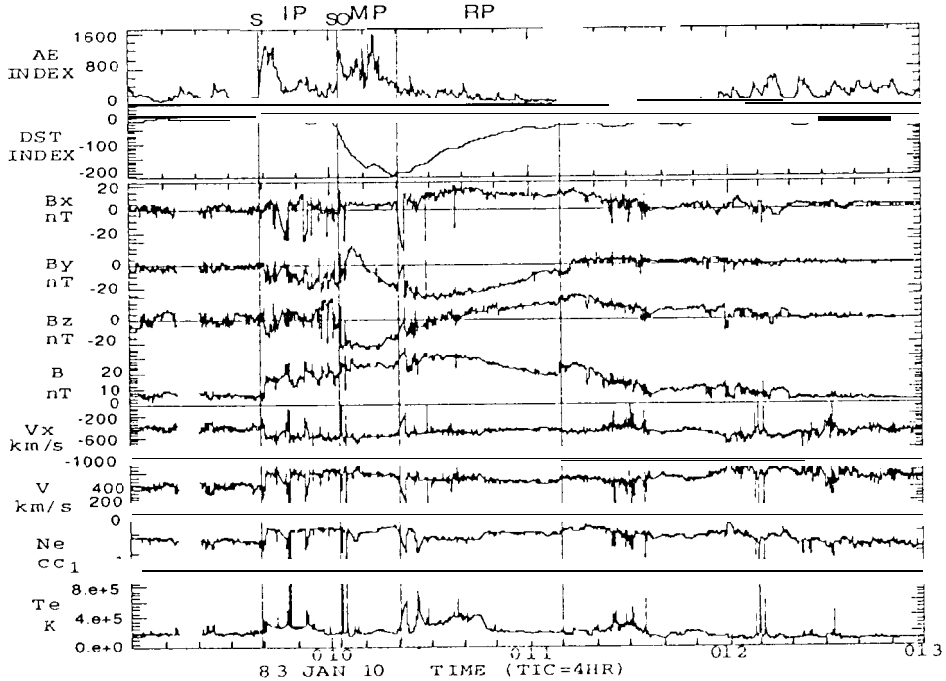
S
IP
SO
MP
RP
AE INDEX
1600
800
0
DST INDEX
0
-100
-200
Bx nT
20
0
-20
By nT
0
-20
Bz nT
0
-20
B nT
20
10
0
Vx km/s
-200
-600
-1000
V km/s
400
200
0
Ne cc1
Te K
8.e+5
4.e+5
0.e+0
010
011
012
013
83 JAN 10
TIME (TIC=4HR)

Fig 2

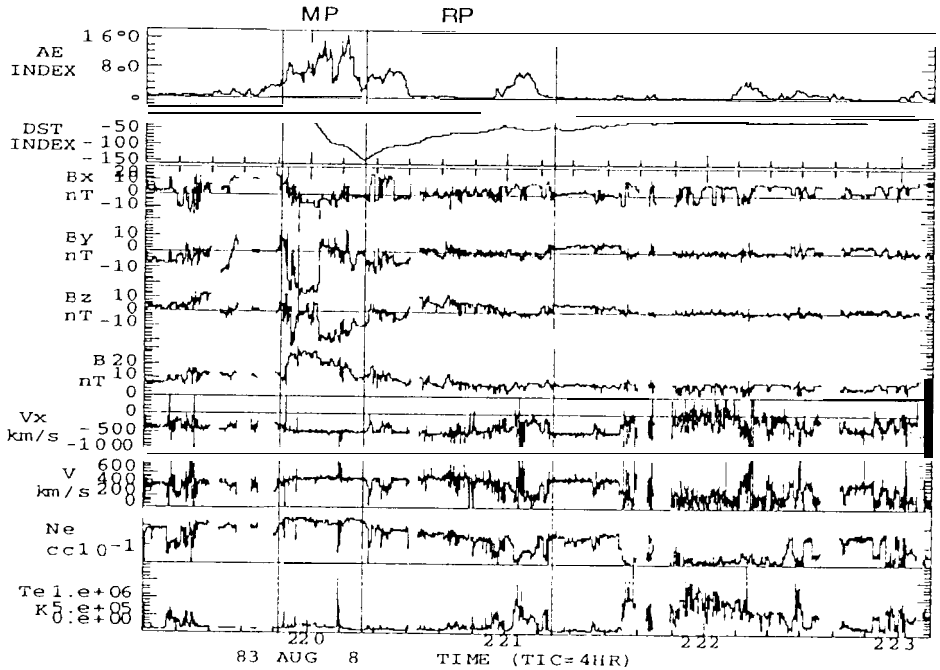
MP
RP
AE INDEX
DST INDEX
Bx nT
By nT
Bz nT
B nT
Vx km/s
V km/s
Ne cc
Te K
220
221
222
223
83 AUG 8
TIME (TIC=4HR)

Fig. 3

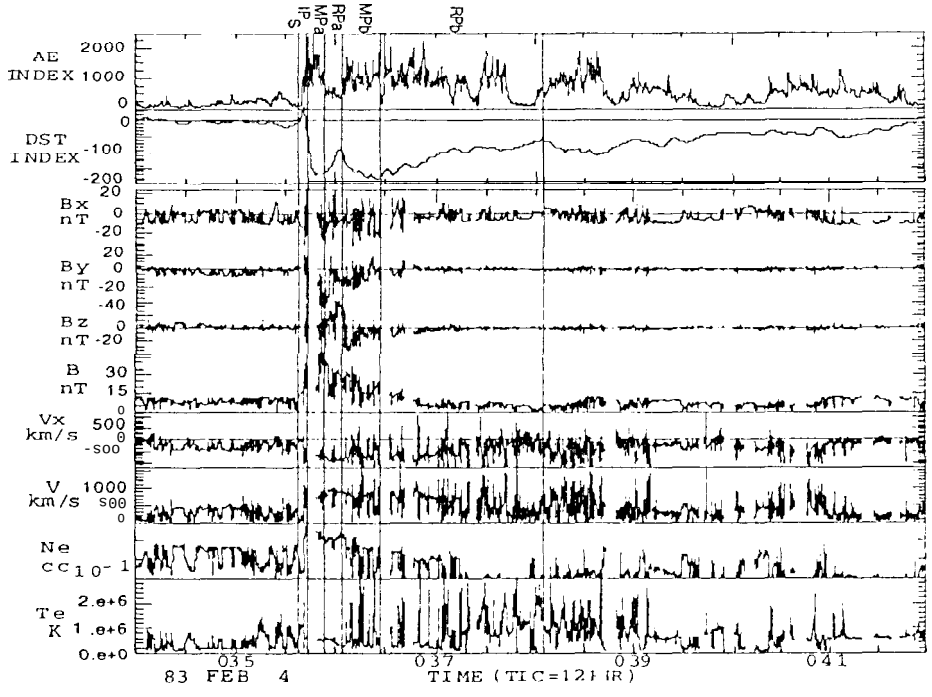
IP
S
MPa
RPa
MPb
RPb
AE INDEX
2000
1000
0
DST INDEX
0
-100
-200
Bx nT
20
0
-20
By nT
20
0
-20
-40
Bz nT
0
-20
B nT
30
15
0
Vx km/s
500
0
-500
V km/s
1000
500
0
Ne cc
10^1
Te K
2.e+6
1.e+6
0.e+0
035
037
039
041
83 FEB 4
TIME (TIC=12 HR)

Fig. 4

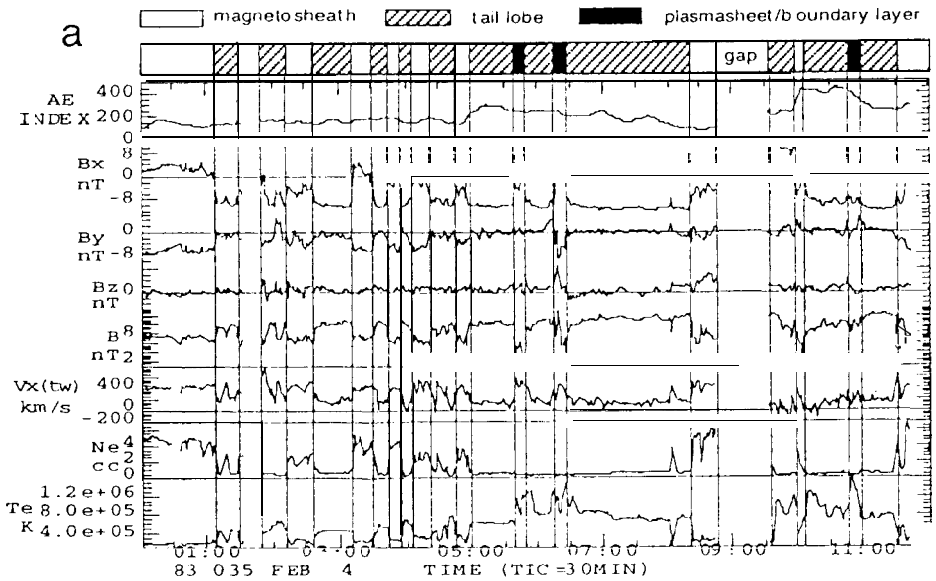
a
magnetosheath
tail lobe
plasmasheet/boundary layer
gap
AE INDEX 400 200 0
Bx nT 8 0 -8
By nT 0 -8
Bz nT 0
B nT 8 2
Vx(tw) km/s 400 0 -200
Ne cc 4 2 0
Te K 1.2e+06 8.0e+05 4.0e+05
01:00
03:00
05:00
07:00
09:00
11:00
83 035 FEB 4
TIME (TIC=30MIN)

Fig. 5a

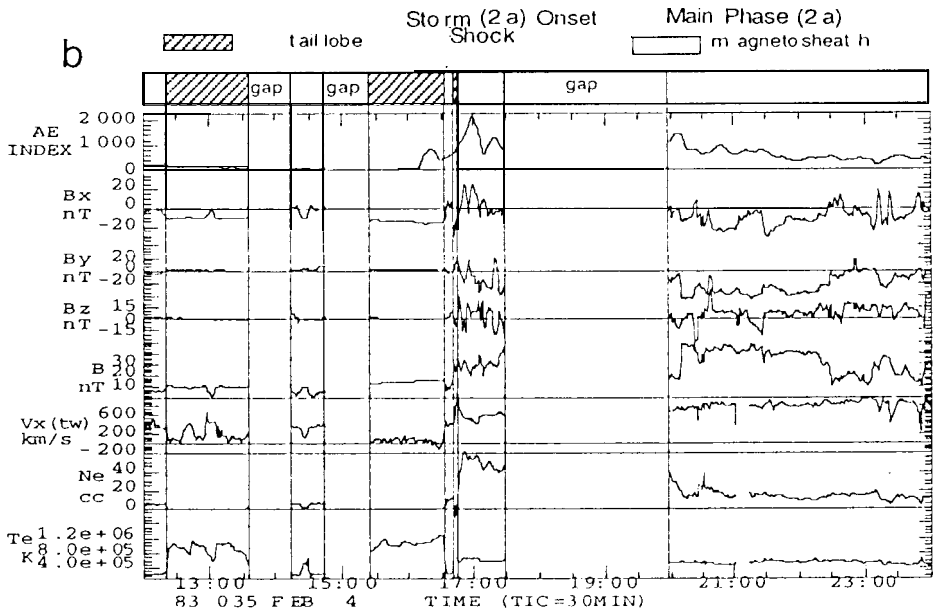
b
tail lobe
Storm (2a) Onset
Shock
Main Phase (2a)
magnetosheath
gap
gap
gap
AE INDEX
2 000
1 000
0
Bx nT
20
0
-20
By nT
20
0
-20
Bz nT
15
0
-15
B nT
30
20
10
Vx(tw) km/s
600
200
- 200
Ne cc
40
20
0
Te K
1.2e+06
8.0e+05
4.0e+05
13:00
15:00
17:00
19:00
21:00
23:00
83 035 FEB 4
TIME (TIC=30MIN)

Fig. 5b

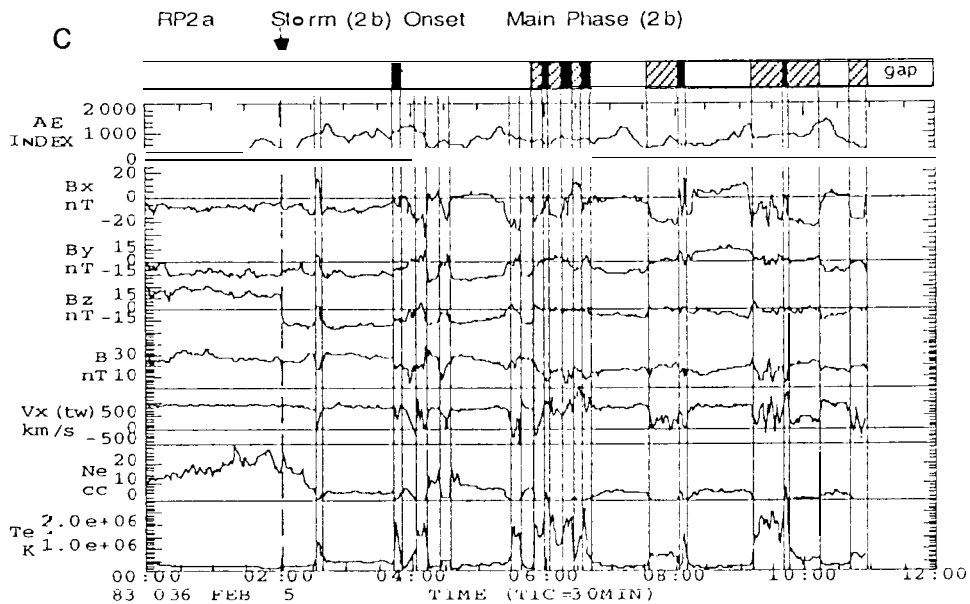
C
RP2a
Storm (2b) Onset
Main Phase (2b)
gap
AE INDEX
2000
1000
0
Bx nT
20
0
-20
By nT
15
0
-15
Bz nT
15
0
-15
B nT
30
10
Vx (tw) km/s
500
0
-500
Ne cc
20
10
0
Te K
2.0e+06
1.0e+06
00:00
02:00
04:00
06:00
08:00
10:00
12:00
83 036 FEB 5
TIME (TIC=30MIN)

Fig. 5c

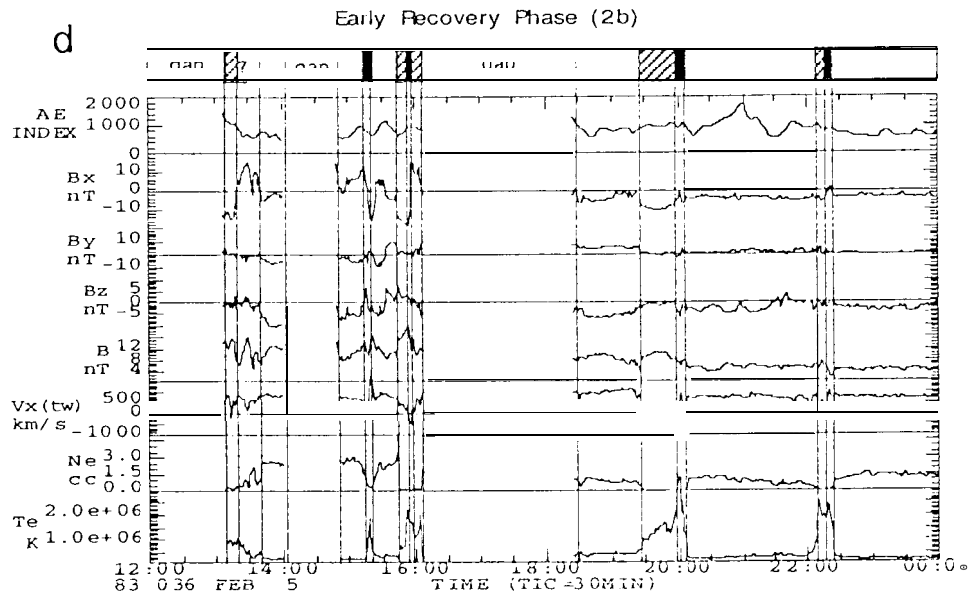
d
Early Recovery Phase (2b)
AE INDEX
2000
1000
0
Bx nT
10
0
-10
By nT
10
-10
Bz nT
5
0
-5
B nT
12
8
4
Vx(tw) km/s
500
0
-1000
Ne cc
3.0
1.5
0.0
Te K
2.0e+06
1.0e+06
12:00
14:00
16:00
18:00
20:00
22:00
00:0
83 036 FEB 5
TIME (TIC=30MIN)

Fig 3d

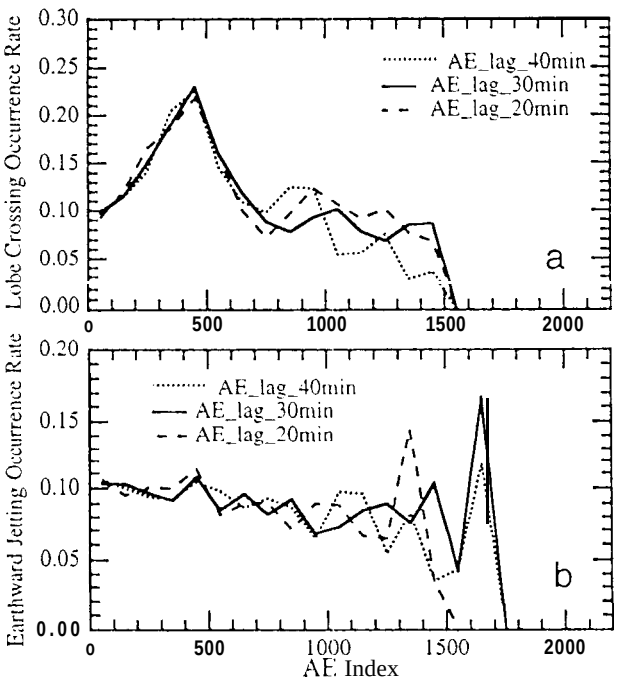
Lobe Crossing Occurrence Rate
0.30
0.25
0.20
0.15
0.10
0.05
0.00
AE_lag_40min
AE_lag_30min
AE_lag_20min
a
0
500
1000
1500
2000
Earthward Jetting Occurrence Rate
0.20
0.15
0.10
0.05
0.00
AE_lag_40min
AE_lag_30min
AE_lag_20min
b
0
500
1000
1500
2000
AE Index

Figure 6

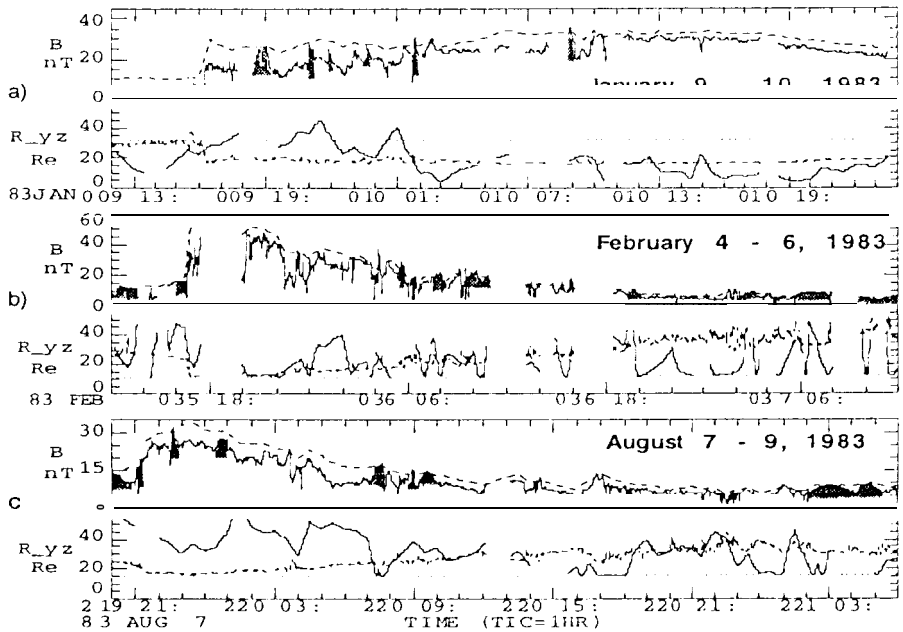
a)
B
nT
40
20
0
R_yz
Re
83JAN 009 13: 009 19: 010 01: 010 07: 010 13: 010 19:
b)
February 4 - 6, 1983
60
83 FEB 035 18: 036 06: 036 18: 037 06:
c
August 7 - 9, 1983
30
15
219 21: 220 03: 220 09: 220 15: 220 21: 221 03:
83 AUG 7
TIME (TIC=1HR)

Fig. 7

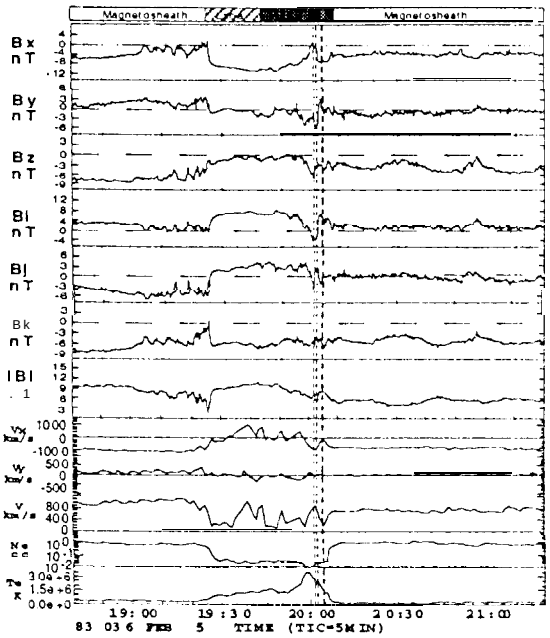
Magnetosheath
Magnetosheath
Bx nT
By nT
Bz nT
Bi nT
Bj nT
Bk nT
|B| . 1
19:00
19:30
20:00
20:30
21:00
83 036 FEB 5 TIME (TIC=5MIN)

Fig. 8

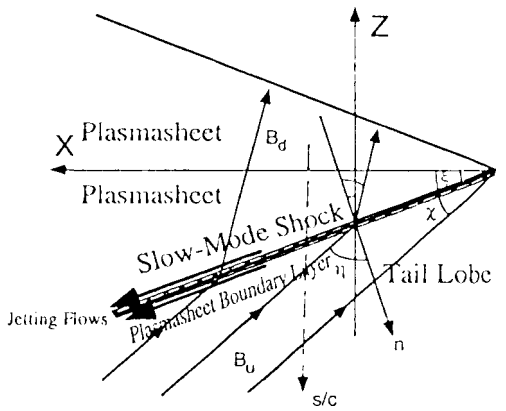
Z
X
Plasmasheet
Plasmasheet
B_d
Slow-Mode Shock
Plasmasheet Boundary Layer
Jetting Flows
Tail Lobe
η
ξ
χ
n
B_u
s/c

Fig. 9